Tuning polymorphism in 2,3-thienoimide capped oligothiophenes based field-effect transistors by implementing vacuum and solution deposition methods

Emilia Benvenuti,*[a] Denis Gentili,*[a] Fabio Chiarella,[b] Alberto Portone,[c] Mario Barra,[b] Marco Cecchini,[d] Chiara Cappuccino,[e] Massimo Zambianchi,[f] Sergio G. Lopez,[a] Tommaso Salzillo,[g] Elisabetta Venuti,[g] Antonio Cassinese,[b] Luana Persano,[d] Dario Pisignano,[c,h] Massimiliano Cavallini,[a] Lucia Maini,[e] Manuela Melucci,[f] Michele Muccini,[a] Stefano Toffanin*[a]

We report on the investigation of the influence of the molecular packing and film morphology on the field-effect charge mobility in 2,3-thienoimide-based oligothiophenes semiconductors (C_n-NT4N). Organic field-effect transistors are realized by implementing both vacuum and solution methods in order to control the solid-state phase of the active layer. Thermal sublimation in high vacuum chamber and Supersonic Molecular Beam Deposition were used as vacuum-based fabrication approaches for preparing thin films, while Lithographically Controlled Wetting was used, as a solution-deposition technique, for the fabrication of microstructured films. Thermal sublimation leads to thin films with a phase packing showing ambipolar behaviour, while Supersonic Molecular Beam Deposition enables, by varying the deposition rate, the formation of two different crystal phases, showing ambipolar and unipolar field-effect behaviours. On the other hand, Lithographically Controlled Wetting enables the formation of C_n-NT4N microstructured active layers and their implementation in field-effect transistors.

[a.] Istituto per lo Studio dei Materiali Nanostrutturati, Consiglio Nazionale delle Ricerche (CNR-ISMN), Via Gobetti 101, 40129 Bologna, Italy
[b.] CNR-SPIN e Dipartimento di Fisica, Università di Napoli Federico II, Piazzale Tecchio 80, 80125 Napoli, Italy
[c.] Dipartimento di Matematica e Fisica "Ennio De Giorgi", Università del Salento, via Arnesano 73100, Lecce, Italy
[d.] NEST, Istituto Nanoscienze-CNR, Piazza S. Silvestro 12, I-56127 Pisa, Italy
[e.] Dipartimento di Chimica "G. Ciamician", Università di Bologna, Via F. Selmi 2, 40126, Bologna, Italy
[f.] Istituto per la Sintesi Organica e la Fotoreattività, Consiglio Nazionale delle Ricerche (CNR-ISOF), Via Gobetti 101, 40129 Bologna, Italy
[g.] Dipartimento di Chimica Industriale Toso Montanari, Università di Bologna, Viale del Risorgimento 4, 40136 Bologna, Italy
[h.] Dipartimento di Fisica, Università di Pisa, Largo B. Pontecorvo 3, I-56127 Pisa, Italy

Introduction

Polymorphism is emerging in organic optoelectronics as a powerful tool, alternative to molecular design, to control the packing dependent functionalities of organic materials, such as optical, charge transport and optoelectronic properties.[1] Polymorphic pentacenes,[2,3] tetrathiafulvalenes[4,5] and rubrene[6] materials have been widely investigated to study the influence of molecular packing on charge transport capability in organic semiconductors. Recently, a clear relationship between polymorph type and p-type mobility was established for fluorinated 5,11-bis(triethylsilylethynyl)anthradithiophene.[7] Similarly, Kim et al. demonstrated polymorphism as a tool to control optoelectronic and charge transport functionalities in two fluorene-based π-conjugated materials,[8] while Wang et al. suggested the possibility of lasing in different colors by exploiting a single polymorphic (4,4'-(thiazolo[5,4-d]-thiazole-2,5-diyl)bis(N,N-diphenylaniline) compound.[9]
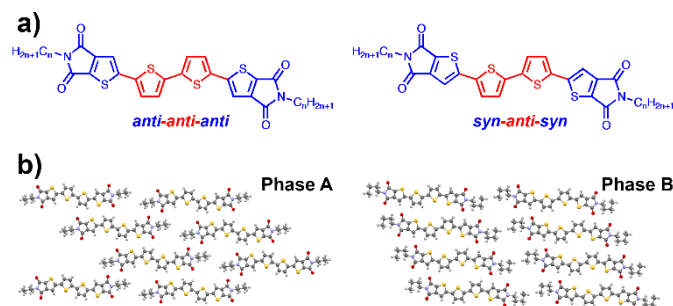

Figure 1. (a) Molecular structure and conformational polymorphism types of the Cn-NT4N semiconductors herein studied; (b) molecular packing.

Tuning the optical, electrical and optoelectronic properties of organic semiconductors through the control of their polymorphic phases is particularly important for organic light emitting transistors (OLETs),[10] whose electronic, optoelectronic and photonic multifunctionality strictly depends on the active material properties under operational conditions.

Thiophene molecular semiconductors are highly versatile organic materials,[11,12] whose properties are representative of a broad range of organic semiconductor materials. 2,3-thienoimide end-capped oligothiophenes, also known as thienopyrrolyldione-based oligothiophenes (C_n-NT4N), show polymorphism[13] and have the peculiarity of combining ambipolar semiconducting capability and electroluminescence, making them suitable materials for the fabrication of both ambipolar organic field-effect transistors (OFETs)[14] and single-layer OLETs.[15] A wide library of C_n-NT4N compounds has been synthesized and characterized to study the

effect of the N-alkyl end shape and size on the optical, self-assembly and charge transport properties.[16] We have recently reported the relationship between molecular structures and polymorphism properties of C_n-NT4N derivatives.[17] Interestingly, C_n-NT4N derivatives with an even number of carbon atoms in the alkyl end chains display at least two conformational polymorphs that adopt different molecular packings, namely phase A and phase B, as a consequence of the different conformational arrangement of the 2,3-thienoimide end-moieties with respect to the adjacent thiophene core, i.e. anti or syn conformation (Figure 1a). Consequently, while form A shows columnar π-stacking packing, phase B shows a brick wall-like packing (Figure 1b).[17] The occurrence of different molecular packings may limit the reproducibility, stability, and reliability of devices based on these materials, therefore, the control of polymorph formation during films deposition is crucial for their applicability.

Herein, we report on the impact of the deposition technique on the charge transport properties of thin and microstructured films of 2,3-thienoimide-based molecular semiconductors and investigate their molecular packing, morphology and optical properties. We have chosen the butyl (C_4-NT4N) and hexyl-ended (C_6-NT4N) oligomers because they are vacuum- and solution-processable semiconductors, respectively, and both exhibit polymorphism. Thermal sublimation in high vacuum chamber and Supersonic Molecular Beam Deposition (SuMBD) were used as vacuum-based fabrication approaches for preparing thin films, while Lithographically Controlled Wetting (LCW) was used, as solution-deposition technique, for the fabrication of microstructured films. We observed that thermal sublimation leads to thin films exhibiting ambipolar behaviour, while SuMBD enables the formation of both ambipolar and unipolar thin films. Ambipolar thin films are characterized by a polymorph B with brick-wall like packing, whereas unipolar thin films exhibit a new molecular packing that hampers the hole transport. We further demonstrate that spatial confinement of solution-deposition of 2,3-thienoimide capped oligothiophene achieved by LCW is an effective strategy for fabricating microstructured films with controlled features and suitable for their implementation in devices, overcoming the shortcomings of inhomogeneous films that are achieved by drop casting and spin coating. Solution-processed films of C_6-NT4N were deposited from both anisole solution at 80 °C and 1,2-dichlorobenzene (1,2-DCB) solution at room temperature. Microstructured films exhibit ambipolar behaviour and are characterized by phase B regardless of the conditions used, while films deposited by drop casting at room temperature adopt the phase A structure, highlighting the key role of spatial confinement in the polymorphism control of wet-deposited C_6-NT4N films.

Results and discussion

Vacuum deposition

Thin films of C_4-NT4N were deposited by both vacuum thermal deposition and SuMBD and used as active layer of OFETs. OFETs were built in a bottom gate/bottom contact architecture using hexamethyldisilazane (HMDS)-treated Si/SiO2 substrates to minimize charge trapping at the interface between the organic semiconductor and the dielectric[18] and to guarantee a more hydrophobic interface suitable for C_n-NT4N growth.

As demonstrated by transfer characteristics in saturation regime (Figure 2a) and summarized in Table 1, thin films of C_4-NT4N deposited at 0.1 Å/s by thermal sublimation exhibit ambipolar field-effect transport with saturated electron and hole mobilities up to 4.5×10^{-2} cm^2 V^{-1} s^{-1} and 6.7×10^{-4} cm^2 V^{-1} s^{-1}, respectively. In agreement with a previous report on C_4-NT4N deposited on PMMA films,[16] XRD analysis reveals that thermal sublimation of C_4-NT4N on HMDS-functionalized silicon dioxide yielded the phase B (Figure S1).
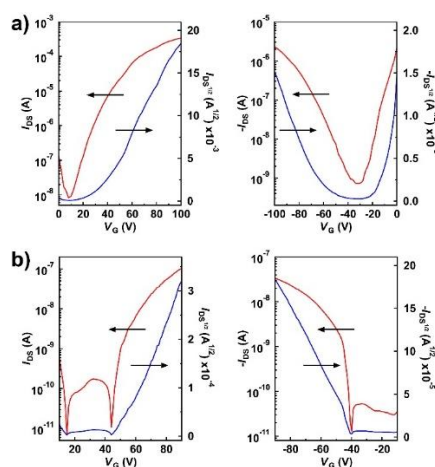

Figure 2. Transfer characteristics measured at positive and negative source–drain bias of representative field-effect transistors based on C_4-NT4N films deposited by thermal sublimation(a) and SuMBD (b) at 0.1 Å/s. (drain voltage $V_{SD} = \pm 100$ V).

Table 1. Electrical data of bottom gate/bottom contact OFETs based on vapour-deposited films of C_4-NT4N

	Rate (Å/s)	Phase	μ_e (cm^2 V^{-1} s^{-1})	V_{th}^e (V)	I_{on}^e/I_{off}^e	μ_h (cm^2 V^{-1} s^{-1})	V_{th}^h (V)	I_{on}^h/I_{off}^h
Sublimation	0.1	B	4.5×10^{-2}	58	10^5	6.7×10^{-4}	-72	10^3
Sublimation	0.017	B	1.2×10^{-2}	61	10^4	1.3×10^{-4}	-67	10^3
SuMBD	0.1	B	1.2×10^{-5}	50	10^4	2.2×10^{-6}	-35	10^3
SuMBD	0.017	C	1.3×10^{-4}	53	10^4	-	-	-

Moreover, considering that the bottom contact configuration is usually characterized by less effective charge injection than the top contact one,[19] also the hole and electron carrier mobilities are in good agreement with what was previously reported.[16] On the other hand, the threshold for electron transport is higher when HMDS-treated SiO$_2$ was used instead of PMMA (i.e. a material with low surface trapping density) as a dielectric layer, confirming that electron traps cannot be completely passivated through the functionalization with HMDS.[18] As reported in Table 1, the field-effect properties are not substantially affected by the decrease of deposition rate, thin films of C_4-NT4N grown by thermal deposition at 0.017 Å/s exhibit ambipolar field-effect transport with mobilities and threshold voltages close to those obtained at higher rate. As revealed by XRD analysis (Figure S1), these results are due to the fact that also at low rate the films are composed of phase B. Beside vacuum thermal deposition, we have also investigated the deposition of C_4-NT4N by SuMBD, which is an effective strategy to activate specific film growth[20] since it allows a good control of the kinetic energy, E_k, of the molecules impinging the growth surface. Highly performing n-type[21] and p-type[22] OFETs have been realized by this method as well as the controlled deposition of different polymorphic phases in titanyl phthalocyanine layers.[23] C_4-NT4N was deposited with a kinetic energy E_k = 12.4 eV, being close to the saturation value that is theoretically predicted to be 13 eV. This feature induces a growth regime very far from the equilibrium, where the roto-vibrational degrees of freedom of the molecules are frozen. C_4-NT4N films deposited at 0.1 Å/s by SuMBD exhibit ambipolar behaviour, but yielded field-effect electron and hole mobilities in saturation regime of 1.2×10^{-5} cm^2 V^{-1} s^{-1} and 2.2×10^{-6} cm^2 V^{-1} s^{-1}, respectively, thus two orders of magnitude lower than what is observed for films deposited at the same deposition rate by thermal sublimation (Figure 2b and Table 1). Nevertheless, XRD measurements reported in Figure 3b show that, in agreement with what was obtained with thermal deposition, the thin films of C_4-NT4N deposited by SuMBD at 0.1 Å/s consist of phase B. Therefore, the difference in electrical performance between films deposited by thermal sublimation and SuMBD can be explained in terms of film morphology. Indeed, the film morphology assessed by AFM reveals that thin films deposited by thermal sublimation are characterized by growth of tridimensional crystals on continuous layers independently of deposition rate (Figure 4a, b). In contrast, the morphology of thin films deposited by SuMBD is characterized by the coexistence of small grains with a lateral size lower than 100 nm and tridimensional structures (Figure 4c). To investigate the effect of the deposition rate, we have also studied the field-effect properties of thin films deposited by SuMBD at a lower deposition rate, i.e. 0.017 Å/s. In sharp contrast to the films deposited at 0.1 Å/s, thin films of C_4-NT4N grown at low deposition rate show only n-type field-effect response with a maximum mobility of about 10^{-4} cm^2 V^{-1} s^{-1} (Figure 3a and Table 1) and are characterized by rounded and well-defined terraced grains with steps close to 2 nm, i.e. comparable with the length of C_4-NT4N molecule (Figure 4d). As shown in Figure 3b, the XRD pattern of thin films deposited at 0.017 Å/s displays a unique peak at low angles (about 4.8°) that is not compatible with either phase A or B, revealing the presence of a polymorph with a different crystal structure, namely phase C. Therefore, as previously observed for other organic semiconductors,[24,25] the absence of p-type behaviour can be ascribed to skeletal distortions of C_4-NT4N molecules in the molecular packing of phase C that disrupt π-conjugation, as also supported by Raman and photophysical characterization (see below), and hinder the hole transport.
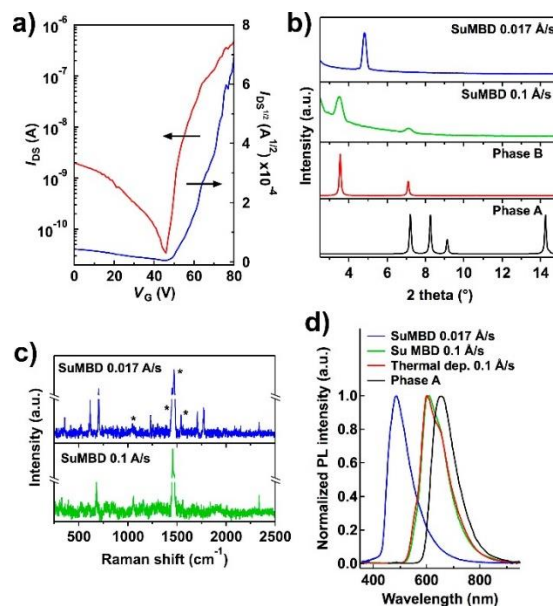
Figure 3. (a) Transfer characteristics measured at positive source–drain bias of a representative field-effect transistor based on a C_4-NT4N film deposited by SuMBD at 0.017 Å/s. (drain voltage V_{SD} = 100 V). (b) XRD patterns of the C_4-NT4N thin films deposited on HMDS-treated Si/SiO$_2$ by SuMBD at 0.1 (green line) and 0.017 Å/s (blue line), and calculated diffractograms of A (black line) and B (red line) phases. (c) Raman spectra of C_4-NT4N thin films deposited on HMDS-treated Si/SiO$_2$ by SuMBD at 0.1 (green line) and 0.017 Å/s (blue line). (d) PL spectra of C_4-NT4N thin films deposited on quartz by SuMBD at 0.017 Å/s (blue line) and at 0.1 Å/s (green line), and by thermal sublimation at 0.1 Å/s (red line), and C_4-NT4N (phase A) powder (black line).

As shown in Figure 3c, Raman spectra of the thin films deposited by SuMBD with different deposition rates show different bands. The films grown at 0.1 Å/s are characterized by the specific Raman pattern, ranging between 1100 and 1400 cm^{-1}, previously assigned to the B phase packing of the C_n-NT4N molecules, whereas the films deposited at 0.017 Å/s do not show in the same spectral region the Raman features of either phase A or B.[26] However, their spectrum displays the bands characteristic of the C_n-NT4N molecules (see marks in the Figure 3), revealing that the C_n-NT4N chemical identity after the SuMBD process is fully preserved and thus confirming that the films consist of a new polymorph with a different molecular packing, i.e. the phase C packing.[26] Interestingly, the Raman band of the phase C corresponding to the out of phase C=C stretching mode ($\sim$1500 cm^{-1}),[27] which mainly involves displacements in the outermost rings of the oligothiophene skeleton, is shifted towards higher frequency than that of the other phases. This is likely the indication of a lowering in the conjugation length that can be ascribe to a reduced planarity of the molecular structure. Unfortunately, attempts to obtain pure phase C in bulk were unsuccessful, suggesting that, as previously observed for other organic semiconductors,[28] this polymorph might exist only in thin films.
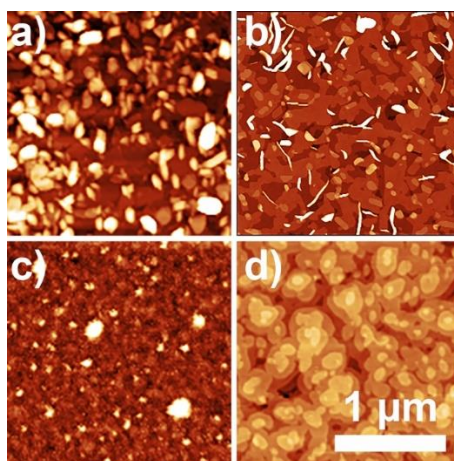

Figure 4. AFM images of C_4-NT4N films deposited on HMDS-treated Si/SiO$_2$ by thermal sublimation at (a) 0.1 Å /s (z-scale: 0-60 nm) and (b) 0.017 Å /s (z-scale: 0-30 nm), and SuMBD at (c) 0.1 Å /s (z-scale: 0-15 nm) and (d) 0.017 Å /s (z-scale: 0-15 nm).

The optical properties of C_4-NT4N films were investigated by photoluminescence spectroscopy. The PL spectra of thin films of C_4-NT4N deposited at 0.1 Å/s by both vacuum thermal deposition and SuMBD reveal the characteristic emission features expected for phase B,[17] consisting of an emission band centered at about 600 nm (Figure 3c, red and green lines). In sharp contrast, films of C_4-NT4N deposited at 0.017 Å/s by SuMBD show an emission band centered at 488 nm and, thus, blue-shifted compared to the characteristic PL emission of A and B polymorphs of C_4-NT4N (Figure 3c, blue line).[17] Therefore, in good agreement with the XRD and Raman measurements, the photophysical properties indicate that thin films of C_4-NT4N obtained at 0.017 Å/s by SuMBD are composed of a new phase in which, probably due to the energetics of the supersonic beam, the molecular moieties are arranged in a sterically hindered configuration so that the π-π delocalization in the crystalline domains is reduced. However, as demonstrated by the electrical characterization, the molecular moieties arrange according to a solid-state configuration that preserves an efficient overlapping of π orbitals[29] to allow the lateral electron transport in FET devices.

Solution deposition

Previous studies carried out by our group demonstrated that both drop casting and spin coating of solution of C_n-NT4N molecules leads to the formation of needle shaped microcrystals unsuitable for the fabrication of OFETs.[17] In light of that, we have exploited an unconventional wet lithographic technique, i.e. Lithographically Controlled Wetting (LCW), to pattern and study the electrical properties of C_6-NT4N, as it is the most soluble of the C_n-NT4N series.[17]
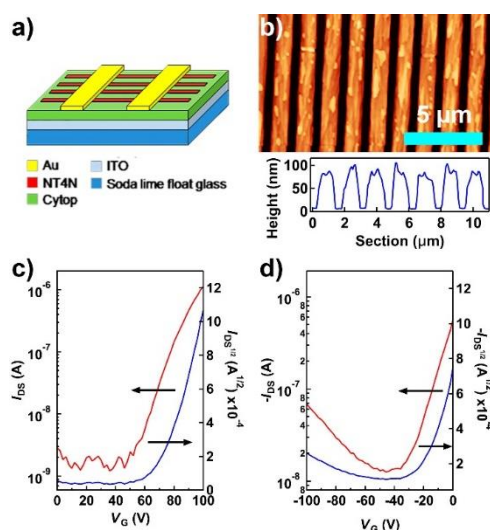

Figure 5. (a) Schematic representation of a bottom gate/top contact OFET based on C_6-NT4N microstripes. (b) AFM image of C_6-NT4N depositated on Cytop by LCW from anisole solution (z-scale: 0-150 nm) and corresponding profile. Transfer characteristics measured at positive or negative source–drain bias of a representative field-effect transistor based on C_6-NT4N deposited by LCW from (c) anisole and (d) 1,2-DCB solution (drain voltage V_{SD} = ±100 V).

Table 2. Electrical data of bottom gate/top contact OFETs based on solution-deposited films of C_6-NT4N

	Solvent	Phase	μ_e ($cm^2V^{-1}s^{-1}$)	I^e_{on}/I^e_{off}	V_{th}^e (V)	μ_h ($cm^2V^{-1}s^{-1}$)	V_{th}^h (V)	I^h_{on}/I^h_{off}
LCW	Anisole	B	2.4×10^{-3}	10^3	62	1.0×10^{-5}	-56	10^1
LCW	1,2-DCB	B (A)	4.4×10^{-4}	10^2	60	2.7×10^{-5}	-64	10^1
Sublimation	-	B	2.0×10^{-1}	10^4	57	2.2×10^{-3}	-68	10^3

LCW is a stamp-assisted technique that exploits the self-organizing properties of the materials in a spatially confined system for creating micro and nanostructured thin films replicating the stamp features. LCW has been successfully employed for the integration of soluble organic and metal-organic compounds in OFETs.[30,31] Since attempts to implement microstructured films in bottom gate/bottom contact transistors were unsuccessful, OFETs based on microstripes of C_6-NT4N were fabricated by LCW in a bottom gate/top contact configuration, i.e. the best performing configuration for Cn-NT4N based device,[16] using a perfluorinated polymer (Cytop) as dielectric layer to guarantee the solvent orthogonality (Figure 5a). All the steps of fabrication were performed under controlled atmosphere in order to prevent degradation phenomena activated by oxygen and water. As shown in Figure 5b, C_6-NT4N microstripes (~80 nm high) with controlled size, shape, and orientation were successfully fabricated by LCW using anisole

solution at 80 °C and 1,2-dichlorobenzene (1,2-DCB) as solvent at room temperature. The temperature was optimized in order to enhance the solubility and allow the formation of long-range molecular ordered stripes.

Figure 5c, d and Figure S2 show the transfer and output characteristics of the C_6-NT4N based devices fabricated by LCW. The output characteristics curves exhibit superimposition of standard saturation behaviour for one charge carrier and a superlinear current increase due to injection of the other charge carrier, indication of the typical ambipolar transport behaviour expected for C_6-NT4N. In Table 2 the electrical performance of the devices fabricated both by LCW and, for comparison, by thermal sublimation of C_6-NT4N (Figure S3) are summarized. All the devices exhibit unbalanced field-effect charge transport, but solvent-processed microstructured C_6-NT4N films yielded lower field-effect performance than vapor-deposited films. Microstripes of C_6-NT4N deposited from anisole solution exhibit electron and hole mobilities in saturation regime of 2.4×10^{-3} cm^2 V^{-1} s^{-1} and 1.0×10^{-5} cm^2 V^{-1} s^{-1}, respectively, but using 1,2-DCB solution electron mobility decreases by one order of magnitude. Noteworthy, thin films of C_6-NT4N deposited on Cytop by thermal sublimation showed electrical performance (Table 2) similar to those that have been reported using PMMA as a dielectric layer.[16] XRD analysis shows that microstructured films of C_6-NT4N deposited from anisole solution are characterized by only polymorph B, while the XRD pattern of films deposited from 1,2-DCB solution displays a profile with a doublet for peak at $2\theta \sim 6.1°$ revealing the coexistence of both A and B phases (Figure 6a). In addition, it shows two not identified and correlated peaks at $2\theta = 2.2°$ and $4.4°$ (respectively d = 44.6 and 22.3 Å) that possibly refer to the same family of crystalline planes. Noteworthy, the similarity between the peak at $2\theta = 4.4°$ with the peak at $2\theta = 4.8°$ of the phase C of C_4-NT4N (Figure 3b) suggests the presence of a polymorph of C_6-NT4N with a similar molecular packing. Therefore, this mixed composition of phases may explain the worse performance of microstructured films of C_6-NT4N deposited from 1,2-DCB solution.

To investigate the role of spatial confinement on the selection of phase packing, XRD analysis of C_6-NT4N solution-cast films was performed. As expected, after solvent evaporation C_6-NT4N forms needle shaped microcrystals, but while crystals deposited from anisole solution at 80 °C exhibit a XRD profile compatible with phase B, crystals achieved from 1,2-DCB solution at room temperature exhibit the phase A (Figure S4). Similarly, it has been previously reported that crystals of C_6-NT4N prepared from toluene solution at room temperature are characterized by phase A, but after thermal treatment, the conversion to phase B occurs.[17] Therefore, considering that the two phases are enantiotropically related and, at room temperature, the stable phase is A,[17] our results suggest that the formation of phase B in microstructured films of C_6-NT4N deposited using anisole at 80 °C can be mainly ascribed to the thermal treatment, differently, in the case of microstructured films deposited at room temperature from 1,2-DCB solution, the preferential growth of phase B is induced by the spatial confinement.[32]
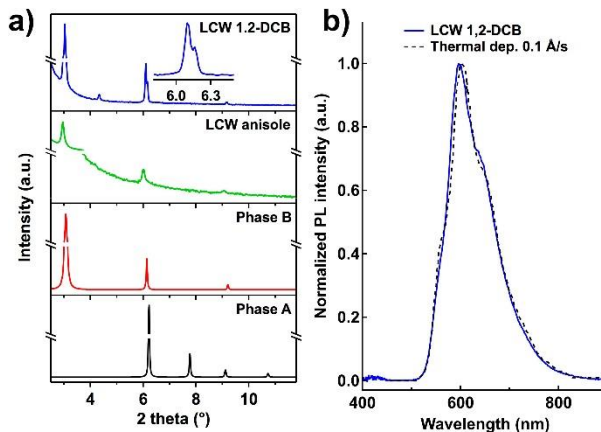

Figure 6. (a) XRD patterns of the C_6-NT4N microstripes deposited on Cytop by LCW from 1,2-DCB (blue line) and anisole (green line) solution, and calculated diffractograms of A (black line) and B (red line) phases. (b) PL spectra of C_6-NT4N micristripes deposited on Cytop by LCW from 1,2-DCB (blue line) and C_6-NT4N thin film deposited on Cytop by thermal sublimation at 0.1 Å/s (black dashed line).

Noteworthy, photoluminescence spectroscopy showed that C_6-NT4N microstripes depositated on Cytop by LCW from 1,2-DCB solution exhibit the emission profile of the phase B (Figure 6b) as also confirmed by localized emission spectra collected in different areas of the microstructured film (Figure S5). We point out that the intensity of the PL spectra is correlated not only to the amount of emissive material present in the film, but also to the PL quantum yield of each phase, which is likely at the base of the difficulty to optically unveil phase A in the microstructured material.

Experimental

Materials

C_n-NT4N compounds were synthesized according to the literature.[17] Hexamethyldisilazane (HMDS) and spectroscopic grade quality solvents were purchased from Sigma-Aldrich. Sylgard 184 (polydimethylsiloxane, PDMS) silicone elastomer base and curing agent were purchased from Dow Corning. CYTOP CTL-809M was purchased from AGC chemicals.

Device fabrication

Bottom gate/bottom contact transistors were fabricated on heavily n-type doped silicon (100) wafers with a 200 nm thermally grown silicon dioxide dielectric layer (C_i = 17.25 nF cm^{-2}). Gold source-drain electrodes (100 nm thick) with width/length ratio of 550 were deposited by vacuum evaporation and patterned by photolithography. Before deposition of semiconductor, the substrates were cleaned by sonication in acetone for 10 min, then in 2-propanol for 10 min, and functionalized with HMDS.[33]

Bottom gate/top contact transistors were fabricated on glass/ITO/Cytop substrates where ITO and Cytop (450 nm) were used as the gate electrode and gate dielectric, respectively. Before deposition of Cytop, the substrates were cleaned by ultrasonic baths in acetone, then 2-propanol and dried under a nitrogen flow. Gold source-drain electrodes (70 nm thick) were deposited by thermal evaporation onto the semiconductor films through a shadow mask at room temperature and 10^{-6} mbar. Devices were fabricated with 12 mm channel width and 70 μm channel length.

Vacuum deposition of ~30 nm thick layers of C_4-NT4N was performed by thermal deposition and SuMBD keeping the substrate at room temperature. The organic precursor vapor for SuMBD was produced in a quartz tube by thermal evaporation with a stagnation pressure of He gas of about 1300 mbar. Molecular vapor was seeded in a supersonic jet of the He carrier gas, resulting in a kinetic energy (E_k) value of the emerging molecular beam of approximately 12.4 eV per molecule.

Solution deposition of C_6-NT4N was performed by LCW.[32] Elastomeric polydimethylsiloxane (PDMS) molds were prepared by replica molding of a Compact Disk supports or silicon masters. The stamp motifs consist of parallel lines 1 μm wide, 230 ± 15 nm deep and 1.7 μm periodicity. After curing for 6 h at 60 °C, PDMS stamps were peeled off, cleaned by sonication in ethanol for 10 min, and dried under nitrogen flow. 5 μL of saturated solution of C_6-NT4N in anisole at 80 °C or 1,2-dichlorobenzene at room temperature were drop casted on the substrate, then a PDMS stamp was placed on the top, paying attention to the stripes orientation, and the solvent was allowed to evaporate under nitrogen for 24 h. For anisole solution, the substrates were heated on a hot plate at 80 °C during film deposition. Afterwards, the stamp was removed and, before characterization, the samples were aged in nitrogen atmosphere for 2 hours.

Electrical Characterization

The electrical measurements were carried out in a MBraun nitrogen glovebox using a standard SUSS probe station coupled to a B1500A Agilent semiconductor device analyser. The field-effect mobility in the saturation regime (μ_{sat}) was calculated using the equation $I_{DS} = (W/2L)C_i\mu_{sat}(V_G - V_T)^2$, where W and L are channel widths and lengths, respectively, C_i is the capacitance per unit area of the insulating layer, and V_T is the threshold voltage extracted from the square root of the drain current ($I_{DS}^{1/2}$) versus gate voltage (V_G) characteristics for a fixed drain voltage (V_{DS}). For solution-processed devices, the effective channel widths were estimated on the basis of the statistical analysis of optical microscopy images.

Optical characterization

Steady-state photo-luminescence (PL) was excited using a CW He–Cd laser at a wavelength of 325 nm and collected under transmission conditions (no color filter was necessary for truncating laser excitation). PL emission was collected using a calibrated optical multichannel analyzer (PMA-11, Hamamatsu). CLSM images of microstructured active layer and localized photoluminescence measurements were carried out with a Nikon Eclipse 2000-E laser scanning confocal microscope using an excitation wavelength of 405 nm.

XRD characterization

X-ray data were collected using a PANalyticalX'Pert PRO diffractometer in Bragg-Brentano configuration equipped with a X'Celerator detector with Cu Kα (λ = 1.5418 Å) as the incident radiation. Soller 0.04 rad, Anti-scatter slit 1/8, divergence slit 1/16, step size 0.017°.

Raman characterization

Raman spectra were recorded with the Renishaw System InVia spectrometer equipped with a Peltier cooled CCD. The spectrometer was coupled to a Leica DLML microscope equipped with 50x, 20x and 5x objectives which allowed for a spatial resolution of about 1 µm with the 50x objective and a nominal field depth ranging from about 25 to 450 µm. The excitation was from a diode laser tuned at 785 nm with a nominal power of 500 mW. The power was reduced by neutral density filters to avoid sample damage.

Morphology measurements

AFM images were collected at room temperature in air on a Multimode 8 microscope operated in PeakForce mode and equipped with a type J scanner (Bruker Nano Inc. GmbH) and SNL-A probes with a nominal spring constant of 0.35 N/m (Bruker AFM Probes, Camarillo, CA), or on an XE-100 microscope operated in non-contact mode (Park Systems) and equipped with a silicon nitride cantilever (Nanosensors). Background interpolation was performed with Gwyddion 2.48 (http://gwyddion.net/).

Conclusions

In this study, we have investigated the impact of the processing method in controlling the polymorphism of two 2,3-thienoimide-based oligothiophenes semiconductors (C_4- and C_6-NT4N) that are typically implemented in the fabrication of multifunctional field-effect transistors. Giving the possibility of C_n-NT4N derivatives to be processed by both vacuum and solution methods, polymorphism was probed and revealed by choosing different deposition techniques, i.e. thermal sublimation, SuMBD and LCW. While thermal sublimation leads to phase B showing an ambipolar behaviour, SuMBD enables, by varying the deposition rate, the formation of both phase B and a new form, named C, showing unipolar field-effect behaviour. Moreover, comparing thin films with the same molecular packing, but deposited by different techniques, we highlighted the fundamental role of film morphology on their electrical performance.

On the other hand, the use of a stamp-assisted technique such as LCW was fundamental in the fabrication of a device since it enables the realization of a microstructured active layer, thus overcoming the inhomogeneity achieved by drop casting and spin coating. In particular, microstructured thin films were deposited from anisole at 80 °C and from 1,2 DCB at room temperature. While drop casting at room temperature leads to phase A, the LCW preferentially leads to phase B, showing the importance of the spatial confinement in controlling the polymorphism. For the first time, we succeeded in demonstrating field-effect charge transport for C_n-NT4N derivative deposited from solution.

In conclusion, our study confirms that the process of deposition, with the control of the polymorph type and the morphological features, may represent a straightforward and effective way to tune the electrical properties of 2,3-thienoimide-ended materials.

Conflicts of interest

There are no conflicts to declare.

Acknowledgements

Notes and references

1   H. Chung and Y. Diao, *J. Mater. Chem. C*, 2016, **4**, 3915–3933.

2   A. Troisi and G. Orlandi, *J. Phys. Chem. B*, 2005, **109**, 1849–1856.

3   D. J. Gundlach, T. N. Jackson, D. G. Schlom and S. F. Nelson, *Appl Phys Lett*, 1999, **74**, 3302–3304.

4   H. Jiang, X. Yang, Z. Cui, Y. Liu, H. Li, W. Hu, Y. Liu and D. Zhu, *Appl. Phys. Lett.*, 2007, **91**, 123505.

5   R. Pfattner, M. Mas-Torrent, I. Bilotti, A. Brillante, S. Milita, F. Liscio, F. Biscarini, T. Marszalek, J. Ulanski, A. Nosal, M. Gazicki-

Lipman, M. Leufgen, G. Schmidt, W. M. Laurens, V. Laukhin, J. Veciana and C. Rovira, *Adv. Mater.*, 2010, **22**, 4198–4203.

6 O. D. Jurchescu, A. Meetsma and T. T. M. Palstra, *Electrochem. Solid-State Lett.*, 2006, **9**, 330–334.

7 O. D. Jurchescu, D. a. Mourey, S. Subramanian, S. R. Parkin, B. M. Vogel, J. E. Anthony, T. N. Jackson and D. J. Gundlach, *Phys. Rev. B*, 2009, **80**, 85201.

8 J. Y. Kim, T. Yasuda, Y. S. Yang, N. Matsumoto and C. Adachi, *Chem. Commun.*, 2014, **50**, 1523–6.

9 K. Wang, H. Zhang, S. Chen, G. Yang, J. Zhang, W. Tian, Z. Su and Y. Wang, *Adv. Mater.*, 2014, **26**, 6168–6173.

10 M. Muccini, W. Koopman and S. Toffanin, *Laser Photonics Rev.*, 2012, **6**, 258–275.

11 Igor F. Perepichka and D. F. Perepichka, *Handbook of Thiophene Based Materials*, 2009.

12 L. Zhang, N. S. Colella, B. P. Cherniawski, S. C. B. Mannsfeld and A. L. Briseno, *ACS Appl. Mater. Interfaces*, 2014, **6**, 5327–5343.

13 M. Zambianchi, L. Favaretto, M. Durso, C. Bettini, A. Zanelli, I. Manet, M. Gazzano, L. Maini, D. Gentili, S. Toffanin, F. Gallino, M. Muccini, M. Cavallini and M. Melucci, *J. Mater. Chem. C*, 2015, **3**, 121–131.

14 M. Durso, C. Bettini, A. Zanelli, M. Gazzano, M. G. Lobello, F. De Angelis, V. Biondo, D. Gentili, R. Capelli, M. Cavallini, S. Toffanin, M. Muccini and M. Melucci, *Org. Electron. physics, Mater. Appl.*, 2013, **14**, 3089–3097.

15 M. Natali, S. D. Quiroga, L. Passoni, L. Criante, E. Benvenuti, G. Bolognini, L. Favaretto, M. Melucci, M. Muccini, F. Scotognella, F. Di Fonzo and S. Toffanin, *Adv. Funct. Mater.*, 2017, **27**, 1–8.

16 M. Melucci, M. Durso, C. Bettini, M. Gazzano, L. Maini, S. Toffanin, S. Cavallini, M. Cavallini, D. Gentili, V. Biondo, G. Generali, F. Gallino, R. Capelli and M. Muccini, *J. Mater. Chem. C*, 2014, **2**, 3448–3456.

17 L. Maini, F. Gallino, M. Zambianchi, M. Durso, M. Gazzano, K. Rubini, D. Gentili, I. Manet, M. Muccini, S. Toffanin, M. Cavallini and M. Melucci, *Chem. Commun.*, 2015, **51**, 2033–2035.

18 L.-L. Chua, J. Zaumseil, J.-F. Chang, E. C.-W. Ou, P. K.-H. Ho, H. Sirringhaus and R. H. Friend, *Nature*, 2005, **434**, 194–9.

19 K. Noda, Y. Wada and T. Toyabe, *Org. Electron.*, 2014, **15**, 1571–1578.

20 K. Walzer, T. Fritz and K. Leo, *Surf. Sci.*, 2006, **600**, 2064–2069.

21 F. Chiarella, T. Toccoli, M. Barra, L. Aversa, F. Ciccullo, R. Tatti, R. Verucchi, S. Iannotta, A. Cassinese, F. Chiarella, T. Toccoli, M. Barra, L. Aversa, F. Ciccullo, R. Tatti and R. Verucchi, *Appl. Phys. Lett.*, 2014, **104**, 143302.

22 Y. Wu, T. Toccoli, N. Koch, E. Iacob, A. Pallaoro, P. Rudolf and S. Iannotta, *Phys. Rev. Lett.*, 2007, **98**, 1–4.

23 N. Coppedè, E. Bonnini, F. Mezzadri, G. Tarabella, P. Ranzieri, L. Barba, G. Arrighetti, L. Lutterotti and S. Iannotta, *Org. Electron. physics, Mater. Appl.*, 2016, **32**, 15–20.

24 A. Facchetti, T. J. Marks and Y. Zheng, *J. Am. Chem. Soc.*, 2010, **132**, 8440–8452.

25 S. Thankaraj Salammal, Z. Zhang, J. Chen, B. Chattopadhyay, J. Wu, L. Fu, C. Fan and H. Chen, *ACS Appl. Mater. Interfaces*, 2016, **8**, 20916–20927.

26 C. Cappuccino, P. P. Mazzeo, T. Salzillo, E. Venuti, A. Giunchi, R. G. Della Valle, A. Brillante, C. Bettini, M. Melucci and L. Maini, *Phys. Chem. Chem. Phys.*, 2018, **20**, 3630–3636.

27 J. Casado, V. Hernandez, R. Ponce Ortiz, M. C. Ruiz Delgado, J. T. Lopez Navarrete, G. Fuhrmann and P. Bauerle, *J. Raman Spectrosc.*, 2004, **35**, 592–599.

28 A. M. Hiszpanski, R. M. Baur, B. Kim, N. J. Tremblay, C. Nuckolls, A. R. Woll and Y. L. Loo, *J. Am. Chem. Soc.*, 2014, **136**, 15749–15756.

29 M. Muccini and S. Toffanin, *Organic Light-Emitting Transistors: Towards the Next Generation Display Technology*, Ed. Wiley-Science, Wise Co-Pubblication, Ed. Wiley., 2016.

30 D. Gentili, F. Di Maria, F. Liscio, L. Ferlauto, F. Leonardi, L. Maini, M. Gazzano, S. Milita, G. Barbarella and M. Cavallini, *J. Mater. Chem.*, 2012, **22**, 20852–20856.

31 A. de la Peña Ruigõmez, D. Rodríguez-San-Miguel, K. C. Stylianou, M. Cavallini, D. Gentili, F. Liscio, S. Milita, O. M. Roscioni, M. L. Ruiz-González, C. Carbonell, D. Maspoch, R. Mas-Ballesté, J. L. Segura and F. Zamora, *Chem. - A Eur. J.*, 2015, **21**, 10666–10670.

32 D. Gentili, F. Valle, C. Albonetti, F. Liscio and M. Cavallini, *Acc. Chem. Res.*, 2014, **47**, 2692–2699.

33 M. Barra, D. Viggiano, P. Ambrosino, F. Bloisi, F. V. Di Girolamo, M. V. Soldovieri, M. Taglialatela and A. Cassinese, *Biochim. Biophys. Acta - Gen. Subj.*, 2013, 1830, 4365–4373.